# Proton charge radius extraction from muon scattering at MUSE using dispersively improved chiral effective field theory

F. Gil-Domínguez,[1,*] J. M. Alarcón,[2,†] and C. Weiss[3,‡]

[1]*Instituto de Física Corpuscular (IFIC) (centro mixto CSIC-UV), Institutos de Investigación de Paterna, C/Catedrático José Beltrán 2, 46980 Paterna, Valencia, Spain*

[2]*Universidad de Alcalá, Grupo de Física Nuclear y de Partículas, Departamento de Física y Matemáticas, 28805 Alcalá de Henares (Madrid), Spain*

[3]*Theory Center, Jefferson Lab, Newport News, Virginia 23606, USA*

(Received 15 June 2023; accepted 25 September 2023; published 27 October 2023)

The MUSE experiment at Paul Scherrer Institute will perform the first measurement of low-energy muon-proton elastic scattering (muon lab momenta 115–210 MeV) with the aim of determining the proton charge radius. We study the prospects for the proton radius extraction using the theoretical framework of dispersively improved chiral effective field theory (DI$\chi$EFT). It connects the proton radii with the finite-$Q^2$ behavior of the form factors through complex analyticity and enables the use of data up to $Q^2 \sim 0.1$ GeV$^2$ for radius extraction. We quantify the sensitivity of the $\mu p$ cross section to the proton charge radius, the theoretical uncertainty of the cross section predictions, and the size of two-photon exchange corrections. We find that the optimal kinematics for radius extraction at MUSE is at momenta 210 MeV and $Q^2 \sim 0.05$–$0.08$ GeV$^2$. We compare the performance of electron and muon scattering in the same kinematics. As a by-product, we obtain explicit predictions for the $\mu p$ and $ep$ cross sections at MUSE as functions of the assumed value of the proton radius.

DOI: 10.1103/PhysRevD.108.074026

## I. INTRODUCTION

The electromagnetic size is a fundamental characteristic of the proton observed in nuclear and atomic physics. It is quantified by the root-mean-squared radii $r_E \equiv \sqrt{\langle r^2 \rangle_E}$ and $r_M \equiv \sqrt{\langle r^2 \rangle_M}$, defined by the derivatives of the electric and magnetic form factors (FFs), $G_E$ and $G_M$, at momentum transfer $Q^2 = 0$, see Ref. [1] for a review. The radii can be determined experimentally either from elastic electron-proton ($ep$) or muon-proton ($\mu p$) scattering or from the nuclear corrections to the energy levels of electronic or muonic hydrogen atoms.

The proton charge radius has been the object of extensive studies in the last decade. The extraction from muonic hydrogen measurements in 2010, $r_E = 0.84184(67)$ fm [2], differed by $5\sigma$ from the CODATA value accepted at the time, $r_E = 0.8768(69)$ fm [3], obtained from electronic hydrogen and electron scattering data ("proton radius puzzle"). The discrepancy motivated experimental and theoretical efforts aiming to improve the extraction methods, quantify the uncertainties, and reconcile the results; see Refs. [4,5] for reviews. The questions raised include the performance of various methods for extraction of the radius from scattering data, the comparison of scattering and atomic results, and potential differences between electron and muon interactions. The cumulative results from these studies tend to favor the "smaller" charge radius. However, one essential piece is still missing—the extraction of the radius from low-energy $\mu p$ elastic scattering.

The MUSE experiment at Paul Scherrer Institute aims to perform the first precise determination of the proton charge radius from $\mu p$ elastic scattering at muon lab momenta 115–210 MeV [6]. Good understanding of the theoretical uncertainties is needed in order to optimize the extraction procedure and assess the final error in the radius. Important questions are the sensitivity of the experimental observables to the proton radius, the theoretical uncertainty in the relation between the proton radius and the finite-$Q^2$ FFs, the size and uncertainty of two-photon exchange (TPE) corrections, and the optimal muon energy and $Q^2$ range for constraining the radius.

The analytic properties of the proton FF play an essential role in the radius extraction from scattering

*fernando.gil@ific.uv.es
†jmanuel.alarcon@uah.es
‡weiss@jlab.org

data. As a function of complex $Q^2$, the form factor has singularities at $Q^2 < 0$, resulting from the $t$-channel exchange of hadronic states (pions, resonances) between the electromagnetic current and the proton. These singularities govern the behavior of the FF at $Q^2 > 0$, where it is measured in scattering experiments. This structure implies a correlation between the derivative of the FF at $Q^2 = 0$ and its values at finite $Q^2$, which is essential for the radius extraction and must be implemented in the theoretical analysis.

The recently developed method of dispersively improved chiral effective field theory (DI$\chi$EFT) [7,8] combines dispersion relations with dynamical input from chiral EFT to describe the nucleon FFs at low $Q^2$ from first principles. It generates FFs with correct analytic properties (position of singularities) and realistic quantitative behavior (strength of singularities), which provide an excellent description of scattering data up to $Q^2 \sim 1$ GeV$^2$ [9]. It also quantifies the theoretical uncertainty of the FF calculations. A special feature of this method is that it generates FF predictions that depend on the assumed proton radius as a parameter. As such it explicitly realizes the correlations between the proton radius and the finite-$Q^2$ behavior of the FF. It permits the use of finite-$Q^2$ data for the radius extraction with controlled uncertainties, which has many experimental and theoretical advantages. The method has been used successfully for the extraction of the proton electric and magnetic radii from electron scattering data [9,10].

In this work we use DI$\chi$EFT to study the prospects for proton radius determination in $\mu p$ elastic scattering at MUSE and optimize the extraction procedure. We compute the $\mu p$ cross section with the DI$\chi$EFT FFs, quantify the theoretical uncertainties and TPE corrections, and evaluate the sensitivity to the proton radius. Specifically, we attempt to answer the following questions:

(1) What is the theoretical sensitivity of the $\mu p$ cross section in MUSE kinematics to the proton radius?
(2) What are the theoretical uncertainties in the $\mu p$ cross section resulting from the DI$\chi$EFT FF predictions and from TPE corrections?
(3) What kinematic range in beam energy and $Q^2$ has the most impact on the radius extraction?
(4) What are the differences between $ep$ and $\mu p$ scattering in radius extraction in MUSE kinematics?

We demonstrate that the radius extraction is characterized by a trade-off between several effects—the sensitivity of the cross section to the radius, the theoretical uncertainty in the FF predictions for a given radius, and the size and kinematic dependence of TPE corrections [9,10]. We determine the optimal kinematics for radius extraction at MUSE based on these considerations. In addition, we provide predictions of the expected $\mu p$ and $ep$ cross sections for the nominal value of the proton radius.

## II. METHODS

### A. Lepton-proton elastic scattering

The elastic lepton-proton scattering process $l(k)+p(p)\to l(k')+p(p')$, where $l = \mu^\mp$ or $e^\mp$, is described by the invariant variables

$$s \equiv (k+p)^2, \qquad Q^2 = -t \equiv -(k-k')^2. \tag{1}$$

In the initial proton rest frame (lab frame), the initial and final muon momenta are $\boldsymbol{k}$ and $\boldsymbol{k}'$, the energies are $\omega \equiv \sqrt{|\boldsymbol{k}|^2 + m^2}$ and $\omega' \equiv \sqrt{|\boldsymbol{k}'|^2 + m^2}$, and the invariants are given by

$$s = M^2 + 2M\omega + m^2, \qquad Q^2 = 2M(\omega - \omega'), \tag{2}$$

where $m$ is the lepton mass and $M$ the proton mass. The scattering angle $\theta_{\rm lab} = \text{angle}(\boldsymbol{k}', \boldsymbol{k})$ is related to the final lepton energy and momentum by

$$\cos\theta_{\rm lab} = \frac{\omega\omega' - m^2 - M(\omega - \omega')}{|\boldsymbol{k}||\boldsymbol{k}'|}. \tag{3}$$

The kinematic range of the momentum transfer accessible at a given initial lepton momentum is

$$0 \le Q^2 \le \frac{4M^2|\boldsymbol{k}|^2}{s} \equiv Q^2_{\rm max}. \tag{4}$$

In the one-photon-exchange approximation, the differential cross section for unpolarized scattering is given by (see, e.g., Ref. [11])

$$\frac{d\sigma_{1\gamma}}{dQ^2} = \frac{\pi\alpha^2}{2M^2|\boldsymbol{k}|^2}\frac{(\epsilon/\tau_P)G_E^2 + G_M^2}{1-\epsilon_T}. \tag{5}$$

Here $\alpha$ is the fine structure constant, and $G_{E,M} \equiv G_{E,M}(Q^2)$ are the electric and magnetic Sachs FFs of the proton. $\epsilon$ is the virtual photon polarization parameter and given by

$$\epsilon = \frac{Q^2_{\rm max} - Q^2 + \frac{m^2}{s}(4M^2+Q^2)}{Q^2_{\rm max} - Q^2 + \frac{Q^2}{2s}(4M^2+Q^2)}, \tag{6}$$

and $\tau_P \equiv Q^2/(4M^2)$. $\epsilon/\tau_P$ is the ratio of the fluxes of longitudinal and transverse polarized photons in the one-photon-exchange approximation. $\epsilon_T$ is the degree of linear polarization of the transverse photons,

$$\epsilon_T = \frac{Q^2_{\rm max} - Q^2}{Q^2_{\rm max} - Q^2 + \frac{Q^2}{2s}(4M^2+Q^2)}, \tag{7}$$

and is bounded by $0 \le \epsilon_T < 1$. In the case of zero lepton mass (as usually assumed in electron scattering) $\epsilon = \epsilon_T$, but for nonzero lepton mass (muon scattering) there are

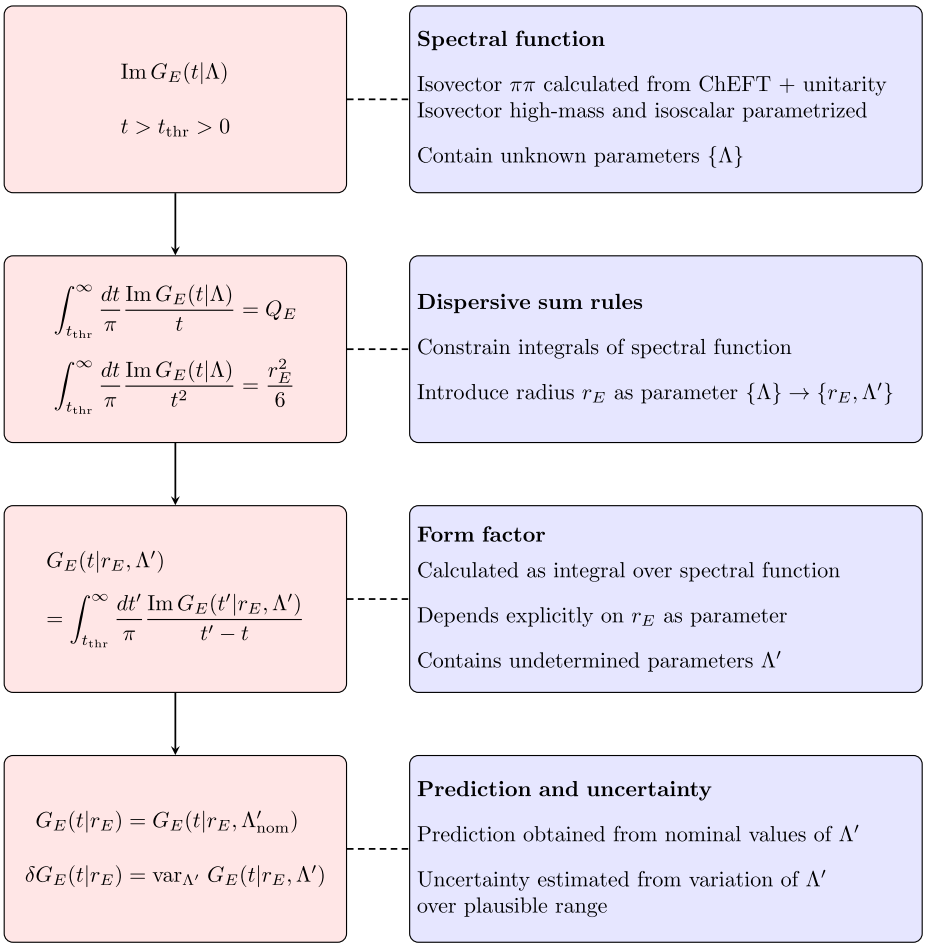


FIG. 1. Flowchart of the DI$\chi$EFT description of the nucleon FFs. Shown is the case of the proton electric FF $G_E$; the same flow applies to the neutron electric FF. In the case of the magnetic FF $G_M$, the right-hand side of the dispersive sum rules is given by the magnetic moment $\mu$ and the magnetic radius $r_M^2$.

important differences. $\epsilon$ attains values $> 1$ at $Q^2 = 0$, and remains nonzero at $Q^2 = Q^2_{\mathrm{max}}$,

$$\epsilon(Q^2 = 0) = \frac{\omega^2}{|\boldsymbol{k}|^2} > 1, \tag{8}$$

$$\epsilon(Q^2 = Q^2_{\mathrm{max}}) = \frac{m^2 s}{2M^2|\boldsymbol{k}|^2} > 0. \tag{9}$$

Two-photon exchange (TPE) corrections play an important role in the analysis of low-energy lepton-proton elastic scattering, see Refs. [12,13] for a review. At order $\alpha^3$, the correction arises from the interference between the two-photon and one-photon exchange amplitudes and is usually included through a multiplicative factor modifying the one-photon exchange cross section,

$$\frac{d\sigma}{dQ^2} \approx \frac{d\sigma_{1\gamma}}{dQ^2}(1 + \delta_{2\gamma}). \tag{10}$$

The correction $\delta_{2\gamma}$ for $\mu p$ scattering has been computed in several theoretical approaches, such as dispersion theory [11,14] and chiral effective field theory [15–17]. In this work we use the results of Ref. [14], which give corrections $\delta_{2\gamma} \lesssim 0.5\%$ in the kinematic range of the MUSE experiment. While in Ref. [14] the inelastic contribution to the dispersion integral for $\delta_{2\gamma}$ was computed in forward kinematics, the analysis of Ref. [11] showed that this approximation is accurate within 10%.

### B. DI$\chi$EFT representation of form factors

The foundations and applications of the DI$\chi$EFT method are described in detail in Refs. [7,8,18]; our implementation in this study follows in particular Ref. [8]. Here we provide a brief summary, emphasizing the aspects relevant to proton radius extraction (information flow, parameters, uncertainties).

DI$\chi$EFT is based on dispersion theory, in which the FFs $G_{E,M}(t)$ at spacelike momentum transfer $t < 0$ are represented as integrals over their imaginary parts $\mathrm{Im}\, G_{E,M}(t)$ on the cut at timelike $t > 0$, the so-called spectral functions. The main steps in the construction of the spectral functions

and the FFs are outlined in Fig. 1. In the following we describe the steps for $G_E$; the ones for $G_M$ are similar.

In the first step, one constructs the spectral function. The proton FF has an isovector and isoscalar component, $G_E \equiv G_E^V + G_E^S$. The isovector FF $G_E^V$ has the two-pion cut at $t > 4M_\pi^2 \equiv t_{\rm thr}$, which dominates the analytic structure at low $t$ and plays an essential role in radius extraction. The isovector spectral function is represented as the sum of two parts,

$$\text{Im } G_E^V(t) = \text{Im } G_E^V(t)[\pi\pi] + \text{Im } G_E^V(t)[\text{high-mass}]. \quad (11)$$

The $\pi\pi$ part covers the region $t_{\rm thr} \le t < t_{\rm max} \approx 1$ GeV$^2$ and is computed theoretically, using the elastic unitarity relation in the $\pi\pi$ channel in the "manifestly real" form (N/D representation) [8]

$$\text{Im } G_E^V(t)[\pi\pi] = \frac{k_{\rm cm}^3}{m_N\sqrt{t}} J_+^1(t) |F_\pi(t)|^2. \quad (12)$$

Here $k_{\rm cm} \equiv \sqrt{t/4 - M_\pi^2}$ is the center-of-mass momentum of the $\pi\pi$ system in the $t$-channel. $|F_\pi(t)|^2$ is the squared modulus of the pion timelike FF. This function contains the full $\pi\pi$ interaction effects and the $\rho$ resonance and is measured in $e^+e^-$ annihilation experiments. $J_\pm^1(t)$ describes the coupling of the $\pi\pi$ system to the nucleon. This function is free of $\pi\pi$ interaction effects (it is real for $t > 4M_\pi^2$) and can be computed in relativistic $\chi$EFT with good accuracy. At low $t \lesssim 10\ M_\pi^2$, $J_\pm^1(t)$ is governed by the Born term singularities of the $\pi N$ amplitudes and known without free parameters. At higher values $t \sim M_\rho^2$, $J_\pm^1(t)$ is subject to higher-order corrections and depends on chiral low-energy constants as free parameters; this dependence allows the height of the spectral function at the $\rho$ peak to vary in a controlled manner and plays an important role in radius extraction (see below). In the present implementation at partial N$^2$LO accuracy [8], it is one single low-energy constant, $\lambda$, that controls the behavior of $J_\pm^1(t)$ at $t \sim M_\rho^2$ and acts as a free parameter.

The high-mass part of the spectral function covers the region $t > 1$ GeV$^2$ and can be parametrized by effective poles. This is justified by the fact that the low–$t$ FF "sees" only the overall spectral strength in the high-mass region, not the details of its distribution (see quantitative assessment below). In the present implementation we use a single effective pole [8]

$$\text{Im } G_E^V(t)[\text{high-mass}] = \pi a_{\rm eff}\delta(t - t_{\rm eff}). \quad (13)$$

The free parameters entering in this part are the pole strength $a_{\rm eff}$ and pole position $t_{\rm eff}$.

The isoscalar FF $G_E^S$ has a three-pion cut, and the spectral function is represented as

$$\text{Im } G_E^S(t) = \text{Im } G_E^S(t)[\pi\pi\pi] + \text{Im } G_E^S(t)[\text{high-mass}]. \quad (14)$$

The $\pi\pi\pi$ part is overwhelmingly concentrated in the $\omega$ resonance and parametrized by a pole $\pi a_\omega \delta(t - M_\omega^2)$. The high-mass part is parametrized by an effective pole, whose position can be taken as the $\phi$ mass, $\pi a_\phi \delta(t - M_\phi^2)$. The free parameters entering in the isoscalar spectral function are the pole strengths $a_\omega$ and $a_\phi$. Altogether, the first step results in a theoretical parametrization of the spectral function of the proton electric form factor

$$\text{Im } G_E(t|\Lambda) = \text{Im } G_E^V(t) + \text{Im } G_E^S(t), \quad (15)$$

where $\{\Lambda\}$ collectively denotes the free parameters. In the present implementation these are $\{\Lambda\} = \{\lambda, a_{\rm eff}, t_{\rm eff}; a_\omega, a_\phi\}$.

In the second step, one imposes the dispersive sum rules for the proton charge and radius

$$\frac{1}{\pi}\int_{t_{\rm thr}}^\infty dt \frac{\text{Im } G_E(t|\Lambda)}{t} = Q_E, \quad (16)$$

$$\frac{1}{\pi}\int_{t_{\rm thr}}^\infty dt \frac{\text{Im } G_E(t|\Lambda)}{t^2} = \frac{r_E^2}{6}, \quad (17)$$

where $Q_E = 1$ is the proton charge and $r_E^2 > 0$ the proton charge radius squared. (The same relations are imposed for the neutron electric FF, in which case $Q_E = 0$ and $r_E^2 < 0$ is the negative neutron charge radius squared.) These relations express the FF at $t = 0$ and its derivative as integrals over the spectral function. One uses them to constrain the parameters in the spectral function. In particular, Eq. (17) is valid for any assumed value of the proton charge radius $r_E$, and one can use it to express one of (or a combination of) the original parameters in terms of the radius, i.e., to introduce the radius as a parameter:

$$\{\Lambda\} \to \{r_E, \Lambda'\}. \quad (18)$$

In this way one obtains a set of spectral functions that depend explicitly on the assumed radius, as well as on the remaining parameters $\Lambda'$

$$\text{Im } G_E(t|r_E, \Lambda'). \quad (19)$$

In the present implementation we use Eqs. (16) and (17) for the proton spectral function (and the same relations for the neutron) to fix the chiral low-energy constant $\lambda$ and the effective pole strengths $a_{\rm eff}, a_\omega, a_\phi$, retaining the isovector effective pole position $t_{\rm eff}$ as the only undetermined parameter.

In the third step, one computes the spacelike FF ($t < 0$, or $Q^2 > 0$) as the dispersion integral with the spectral function,

$$G_E(t|r_E,\Lambda') = \frac{1}{\pi}\int_{t_{\rm thr}}^{\infty} dt' \frac{\mathrm{Im}\, G_E(t'|r_E,\Lambda')}{t'-t}. \quad (20)$$

The FF thus obtained depends on the assumed radius $r_E$ and the undetermined parameters $\Lambda'$. The nominal prediction for the FF with assumed radius $r_E$ is obtained with the nominal values of $\Lambda'$,

$$G_E(t|r_E) = G_E(t|r_E,\Lambda'_{\rm nom}). \quad (21)$$

In the last step, the theoretical uncertainty of the FF with assumed radius $r_E$ is estimated by varying $\Lambda'$ over a plausible range,

$$\delta G_E(t|r_E) = \mathrm{var}_{\Lambda'}\, G_E(t|r_E,\Lambda'). \quad (22)$$

In this way one obtains a nominal prediction and a theoretical uncertainty estimate for the form factor with any given assumed radius. In the present implementation, the undetermined parameter is the position of the isovector high-mass pole. Physical considerations based on $e^+e^-$ annihilation data and the vector meson spectrum suggest the nominal value $t_{\rm eff} = 2.1$ GeV$^2$, and a plausible range of variation for the uncertainty estimate as $t_{\rm eff} =$ 1.4–2.8 GeV$^2$ [10].

Figure 2 shows the resulting FF parametrization for an assumed nominal radius $r_E = 0.84$ fm as a function of $-t = Q^2$ in the kinematic range covered by the MUSE experiment. The lower panel shows the theoretical uncertainty $\delta G_E/G_E$, Eq. (22), estimated from the variation of the high-mass pole position. The upper panel shows the nominal prediction $G_E(t|r_E)$, Eq. (21), for several values of $r_E$ and illustrates the radius sensitivity. One observes: (a) The uncertainty caused by the variation of the high-mass pole position is zero at $t = 0$ and grows quadratically in $-t$ (see lower panel). This is a result of the dispersive sum rules and highlights the "information flow" in the DI$\chi$EFT approach. The FF is constrained by the sum rule Eq. (17) to have a certain first derivative at $t = 0$, given by the assumed radius parameter; any other elements of the parametrization (such as the high-mass poles) can only cause modifications of higher order in $-t$. (b) The uncertainty caused by the variation of the high-mass pole position is of the order $\sim 10^{-3} = 0.1\%$ in the momentum range $|t| \lesssim$ 0.1 GeV$^2$ considered here. This shows the constraining power of the dispersive sum rules, which "project" the information from the radius into the finite-$t$ behavior of the FF. Note that the FF has a nontrivial $t$-dependence and is far from a simple linear behavior in the $t$-range considered here; this can be demonstrated quantitatively by inspecting the higher derivatives and revealing their dynamical scales [18]. (c) The radius sensitivity of the FF is much larger than the uncertainty from the high-mass pole in the $t$-range considered here (see upper panel). A radius variation $\Delta r_E/r_E = \mp 0.01$ causes a change of the FF that is an order of magnitude larger than the estimated uncertainty. This is the basis for the use of the DI$\chi$EFT method for radius extraction from low-$Q^2$ scattering data (see below).

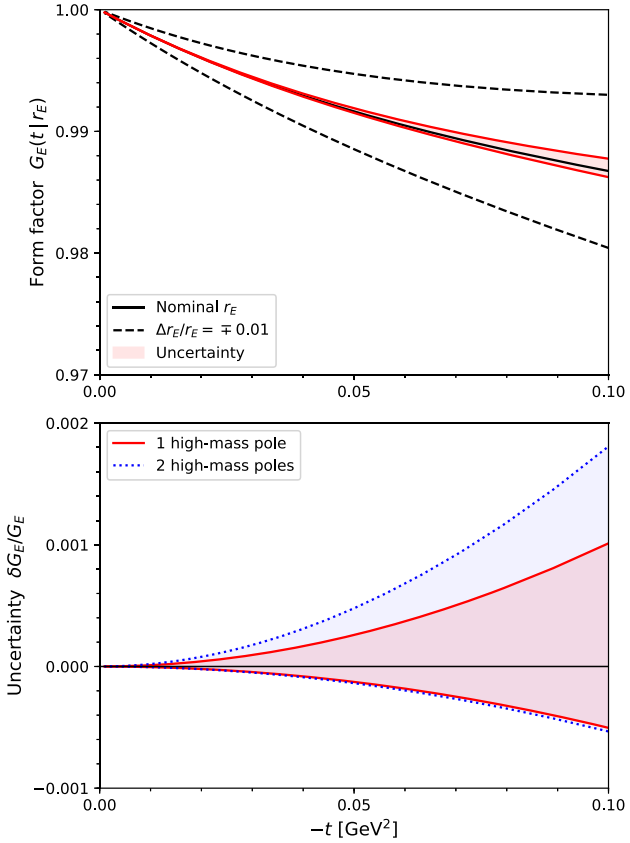


FIG. 2. Radius sensitivity and theoretical uncertainty of the DI$\chi$EFT FF prediction. Lower panel: theoretical uncertainty of DI$\chi$EFT FF prediction estimated with two different parametrizations of the high-mass states (details see text). Solid red lines/shaded red band: One-pole parametrization, Eq. (13). Dotted blue lines/shaded blue band: Two-pole parametrization, Eqs. (23) and (24). Upper panel: DI$\chi$EFT FF prediction for a nominal proton radius $r_E = 0.84$ fm (solid black line) and for radii changed by $\Delta r_E/r_E = \mp 0.01$ (dashed black lines). The shaded red band around the solid line shows the theoretical uncertainty of the FF from the bottom panel (one-pole parametrization). Note that the graphs in the top and bottom panels have different scales on the vertical axes.

The low-$t$ FF predictions (for a given radius) and their estimated theoretical uncertainty are not sensitive to the details of the parametrization of the high-mass states in the spectral function. To demonstrate this quantitatively, we construct the DI$\chi$EFT FF with different parametrizations of the high-mass states and compare the results. As a generalization of the one-pole parametrization Eq. (13), we consider a two-pole parametrization of the form [19]

$$\mathrm{Im}\, G_E^V(t)[\text{high-mass}] = \pi a_{\rm eff}^{(0)} \delta(t - t_{\rm eff}^{(0)}) + \pi a_{\rm eff}^{(1)} \delta'(t - t_{\rm eff}^{(1)}), \quad (23)$$

with pole strengths $a_{\rm eff}^{(0)}$ and $a_{\rm eff}^{(1)}$ and pole positions $t_{\rm eff}^{(0)}$ and $t_{\rm eff}^{(1)}$.[1] In addition to the dispersive sum rules for the charge and radius, Eqs. (16) and (17), we now impose also the sum rule ensuring the $\sim|t|^{-2}$ asymptotic behavior of the spacelike FF at $|t| \to \infty$ (superconvergence relation),

$$\frac{1}{\pi}\int_{t_{\rm thr}}^{\infty} dt\, \mathrm{Im}\, G_E(t|\Lambda) = 0, \tag{24}$$

and use the extended set of sum rules to fix the pole strength parameters. We then estimate the theoretical uncertainty by varying the pole positions $t_{\rm eff}^{(0)}$ and $t_{\rm eff}^{(1)}$ independently over the plausible range 1.4–2.8 GeV$^2$ determined by physical arguments [19]. The two-pole form Eq. (23) covers a much larger range of functional variation in the distribution of high-mass strength than the one-pole form Eq. (13), while being constrained by the same sum rules for the charge and radius. Figure 2 (lower panel) shows the estimated uncertainty. One observes that the uncertainty obtained with the two-pole parametrization has similar magnitude and $t$-dependence to that obtained with the one-pole parametrization, with the range being $\sim$1.5 times larger at $t = -0.05$ GeV$^2$.

Some comments are in order regarding the uncertainty from the high-mass states in our approach. (a) The theoretical uncertainty of the FF prediction (for a given assumed radius) from the high-mass states is not the dominant uncertainty in radius extraction in MUSE kinematics (see Sec. III). A rough estimate of this theoretical uncertainty, as made here, is therefore sufficient. The differences between the high-mass uncertainties estimated with the one-pole and two-pole forms are at the level of "uncertainty of the uncertainty;" they would become relevant to radius extraction only if the other uncertainties could be suppressed to a level that the high-mass uncertainty becomes a limiting factor. (b) The present uncertainty estimates assume that nothing is known about the spectral strength at high masses aside from the dispersive sum rules, which is overly conservative. In fact, data on the spacelike FF at larger $|t| \approx$ 1–2 GeV$^2$ could effectively constrain the high-mass spectral function (within a given parametrization) and reduce the theoretical uncertainty, as is done in empirical dispersive fits to the nucleon FFs [20–22]. We do not take this approach here, as our study focuses on low $|t|$, and we want to treat the functional form of the high-mass spectral function as a theoretical uncertainty, even if it means ignoring certain information. We note that the DI$\chi$EFT method could be combined with an empirical fit to high-$|t|$ FF data in a more comprehensive approach.

[1]The combination of a pole and the first derivative of a pole is effectively equivalent to the sum of two simple poles. The derivative form has the advantage that the pole coefficients have natural size, which helps with understanding their variation in uncertainty estimates.

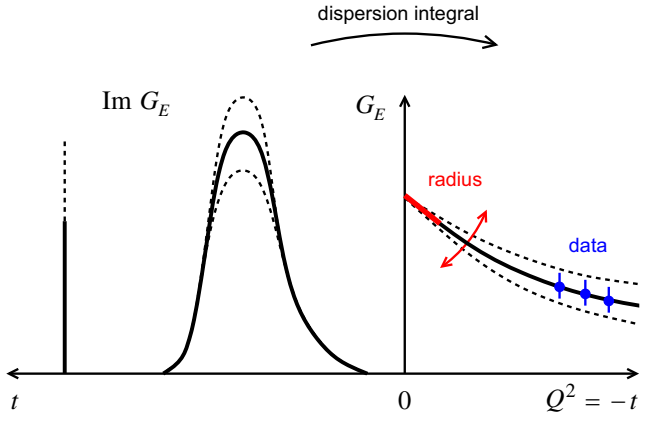


FIG. 3. Illustration of the correlation between the proton radius and the spacelike FF, resulting from analyticity and the information flow in DI$\chi$EFT. The assumed value of the radius constrains the spectral function through the sum rule Eq. (17). The corresponding FF at $Q^2 > 0$ is produced by the dispersion integral Eq. (20). Variation of the radius causes variation of the spectral function and the corresponding FF. (The graph shows only the isovector part of the spectral function at $t > 0$).

The magnetic FF $G_M^V$ and its uncertainty are constructed by an analogous procedure. The dispersive sum rules for $G_M$ now involve the magnetic moment $\mu$ and the magnetic radius $r_M^2$; see Ref. [8] for details. A computer code generating the radius-dependent DI$\chi$EFT FFs $G_{E,M}$ used in the present analysis is available in the Supplemental Materials of Ref. [9].

### C. Proton radius extraction

The DI$\chi$EFT representation of the FFs enables a new theory-guided method of proton radius extraction (see Fig. 3) [9,10]. For each assumed value of the proton radius, the theory generates a spectral function whose features (height of the $\rho$ resonance peak, strength of effective poles) quantitatively depend on the value of the radius. The dispersion integral projects these features into the spacelike region, up to spacelike momentum transfers of the order $Q^2 \sim M_\rho^2$ and beyond. This effectively correlates the assumed value of the radius with the behavior of the spacelike FF at finite $Q^2$ of this order. The correlation described here is based on complex analyticity and the particular information flow in the DI$\chi$EFT calculation and extends far beyond what one could infer from the series expansion in $Q^2$ with a given first derivative. Altogether, this allows one to recruit FF data of the order $Q^2 \sim M_\rho^2$ and beyond for constraining the proton radii.

Radius extraction using DI$\chi$EFT proceeds as follows. For a range of assumed radii, one generates the DI$\chi$EFT FFs as functions of $Q^2$, including their theoretical uncertainties resulting from the undetermined parameters, Eqs. (21) and (22). From these FFs one predicts the cross section for the given assumed radius, including its

theoretical uncertainty from the FFs and two-photon exchange corrections. For a given experimental setup (kinematic coverage, statistical, and systematic errors) one can then assess how data in a given range of energies and $Q^2$ can constrain the radii. The optimal range is determined by a trade-off between the sensitivity of the DI$\chi$EFT FFs to the value of the radius, the theoretical uncertainty of the DI$\chi$EFT FFs, the two-photon exchange effects, and the precision of the data [9,10]. The actual radius can then be determined by a fit in this optimal range, taking into account all the uncertainties. In the following we apply this method to $\mu p$ scattering at MUSE and discuss the prospects for proton radius extraction.

The DI$\chi$EFT method offers several advantages compared to other methods of proton radius extraction. Compared to empirical fits (polynomials, splines), the DI$\chi$EFT method incorporates the analytic structure of the FFs, which includes both the position of the singularities at $t > 0$ and the quantitative distribution of strength in the spectral function. The analytic structure governs the global behavior of the FF, which is difficult to implement in approaches based on polynomial expansions because of strong correlations between higher-order coefficients (analyticity effectively controls the "collective behavior" of higher derivatives of the FF at $Q^2 = 0$ [7]). Compared to traditional dispersion analysis [20–23], the DI$\chi$EFT method allows the strength of the isovector spectral function in the $\rho$ resonance region to vary with the proton radius in a theoretically controlled manner, providing critical flexibility for fitting the spacelike FF data and recruiting them for radius determination. In traditional dispersive fits the $\pi\pi$ part of the isovector spectral function is completely fixed by theory, and the spacelike FF data only constrain the high-mass part of the spectral function, which restricts the interplay of the FF data with the proton radius (the $\rho$ resonance region of the spectral function accounts for about half the value of the proton radius in Eq. (17) [7]).

## III. ANALYSIS

### A. Sensitivity of $\mu p$ cross section to proton radius

We now apply the DI$\chi$EFT framework to study the prospects for proton radius extraction at MUSE. In the first step, we study the sensitivity of the $\mu p$ elastic scattering cross section to the proton electric radius and compare it with the theoretical uncertainties resulting from the DI$\chi$EFT FF predictions, from two-photon exchange corrections, and from the magnetic FF contributions.

To exhibit the various effects, we generate a set of DI$\chi$EFT FF predictions by varying the proton electric radius over the range $r_E = 0.83$–$0.88$ fm in steps $\Delta r_E = 0.01$ fm, and evaluate the $\mu p$ elastic scattering cross section with each of these FFs (the magnetic radius is kept at its nominal value; the role of the magnetic FF in the cross section is discussed below). We include in the cross section the TPE correction of Ref. [14]. Figure 4 shows the predicted cross sections for various incident muon momenta $k \equiv |\boldsymbol{k}|$, as functions of $Q^2$. The lines show the cross section obtained with the nominal DI$\chi$EFT FF predictions for each value of the radius, Eq. (21); the associated bands show the variation due to the theoretical uncertainty of the DI$\chi$EFT FF predictions for the given radius, Eq. (22). The bands at the bottom of the plots show

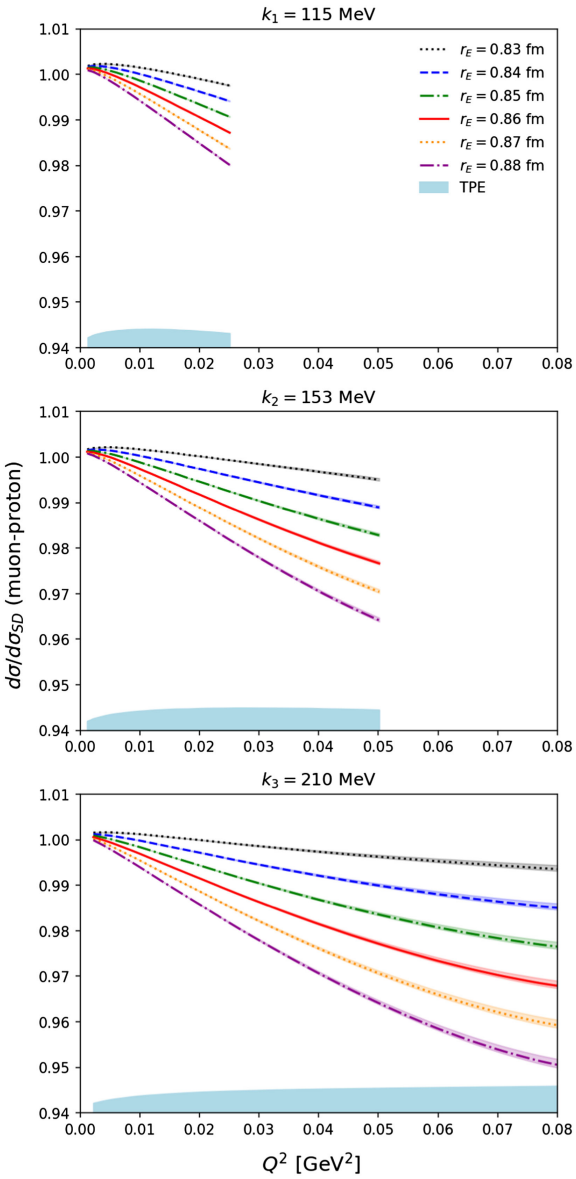


FIG. 4. DI$\chi$EFT predictions for the $\mu^- p$ differential cross section at MUSE for several assumed values of the proton radius. The cross section predictions include the TPE correction, Eq. (10), and are normalized to the standard dipole cross section without TPE effects. Lines (solid, dashed, dotted, dashed-dotted): Nominal DI$\chi$EFT predictions for the assumed value of the proton radius (see legend). Shaded bands around lines: Intrinsic theoretical uncertainty of DI$\chi$EFT predictions, unrelated to assumed proton radius. Shaded band at bottom: TPE contribution to cross section [14].

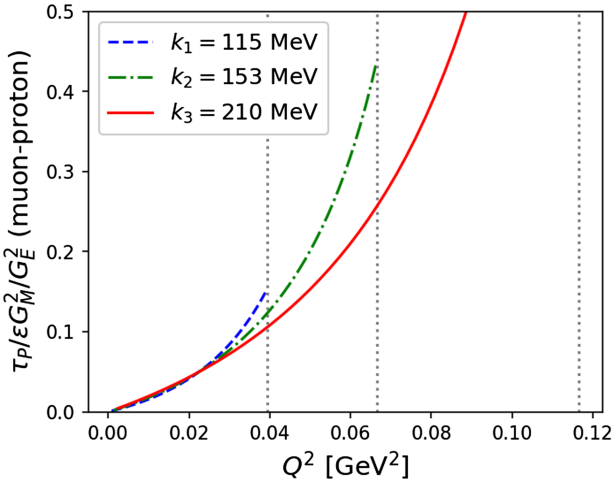


FIG. 5. Ratio of magnetic and electric contributions to the $\mu p$ elastic scattering cross section, $(\tau_P/\epsilon)G_M^2/G_E^2$, in MUSE kinematics. The vertical dotted lines represent the kinematic upper limits of $Q^2$ at the given beam momentum $k$, Eq. (4).

the absolute size of the TPE correction in the cross section predictions (note that this is the overall size of the TPE correction, not its theoretical uncertainty). The standard dipole cross section ($\sigma_{SD}$) used for normalization is the one-photon exchange cross section evaluated assuming the standard dipole $Q^2$-dependence $\propto (1 + Q^2/0.71\ \text{GeV}^2)^{-2}$ for both FFs $G_{E,M}$.

One observes: (a) The sensitivity of the cross section to the proton radius increases with $Q^2$ and with the beam momentum $k$, because the separation of the FF predictions with different radii increases with $Q^2$ [9,10]. At the highest beam momentum, $k = 210$ MeV, the relative variation of the cross section reaches $\Delta\sigma/\sigma \sim 1\%$ for $Q^2$ at the upper end of the range shown here. (b) The theoretical uncertainty of the cross section predictions for given radius also increases with $Q^2$ [9,10]. Overall, the theoretical uncertainty is substantially smaller than the relative variation of the cross section for $\Delta r_E = 0.01$ fm over the kinematic range shown here. (c) The magnitude of the TPE correction does not vary strongly with $Q^2$ and $k$ over the range covered here. At the upper end of the $Q^2$ range, the magnitude of the TPE correction is comparable to the relative variation of the cross section with $\Delta r_E = 0.01$ fm. This clearly shows the importance of the TPE correction for radius extraction.

We also need to consider the uncertainties resulting from the contribution of the magnetic FF to the $\mu p$ elastic scattering cross section. This is particularly important, as with the DI$\chi$EFT framework we can recruit data at higher $Q^2$ for radius extraction, comparable to $Q^2_{\text{max}}$ at the given $k$. Figure 5 shows the ratio of magnetic and electric contributions to the one-photon exchange cross section, $(\tau_P/\epsilon)G_M^2/G_E^2$, in MUSE kinematics. One sees that the ratio depends mainly on $Q^2$, having values $\sim$0.1 at $Q^2 = 0.04$ GeV$^2$ and reaching $\sim$0.4 at $Q^2 = 0.08$ GeV$^2$. Overall, the magnetic contributions to the cross section are limited in all kinematic settings. Using the DI$\chi$EFT framework and the results of the analysis of $ep$ scattering data of Ref. [9], we have computed the effect of the experimental uncertainties of $G_M$ on the $\mu p$ cross section predictions in MUSE kinematics. We observe a maximum variation in the cross sections of the order of 0.04% at the highest $Q^2$, which is small compared to the variation of $\sim$1% resulting from a change of the electric radius $\Delta r_E/r_E = 1\%$. We conclude then that the current experimental uncertainties in $G_M$ do not limit the extraction of the proton electric radius from the $\mu p$ scattering data at the accuracy considered here.

### B. Optimal kinematics for proton radius extraction

In the second step, we discuss the optimal kinematic range for the radius extraction at MUSE. It is determined by the trade-off between the sensitivity of the cross section to the radius, the theoretical uncertainties of the DI$\chi$EFT FF predictions and the TPE corrections, and the experimental errors of the cross section measurement. While the experimental errors can only be estimated at present, some interesting conclusions can already be obtained at this stage.

To make this assessment, we use the difference between the cross section predictions for different radii in Fig. 4 as an estimate of the experimental accuracy required to discriminate between these values of the radii. At each value of $Q^2$ in Fig. 4, we compute the minimal difference between the cross section predictions for radii differing by a given $\Delta r_E$, taking the minimum over all pairs of radii with the given $\Delta r_E$, and taking into account their theoretical uncertainties (i.e., computing the minimal gap between the theoretical uncertainty bands of the cross section predictions for a given $\Delta r_E$). The minimal cross section difference computed in this way is independent of the nominal value of $r_E$. Figure 6 shows the minimal cross section differences obtained in this way, for radius differences $\Delta r_E = 0.01$, 0.02, 0.03 and 0.04 fm, as functions of $Q^2$. One observes: (a) The cross section differences depend strongly on $Q^2$ for fixed $k$. They depend relatively weakly on $k$ for fixed $Q^2$ (when comparing them at a fixed $Q^2$ that is kinematically accessible at multiple values of $k$). The main role of $k$ is to define the kinematically accessible range of $Q^2$. (b) At low values of $Q^2$, high experimental precision is needed for radius determination. At $Q^2 \lesssim 0.015$ GeV$^2$, a relative accuracy $\leq 0.2\%$ is needed for $\Delta r_E = 0.01$ fm, independently of $k$. (c) The demands on the experimental accuracy decrease at higher $Q^2$. At $Q^2 \sim 0.05$ GeV$^2$, a relative accuracy $\sim$0.5% is needed for $\Delta r_E = 0.01$ fm.

Another factor to consider is the uncertainty in the theoretical calculation of the TPE correction [14]. Depending on the kinematics, this contribution to the cross section can be crucial for determining the radius with the necessary precision. Figure 6 compares the value of the TPE correction with the predicted cross section differences

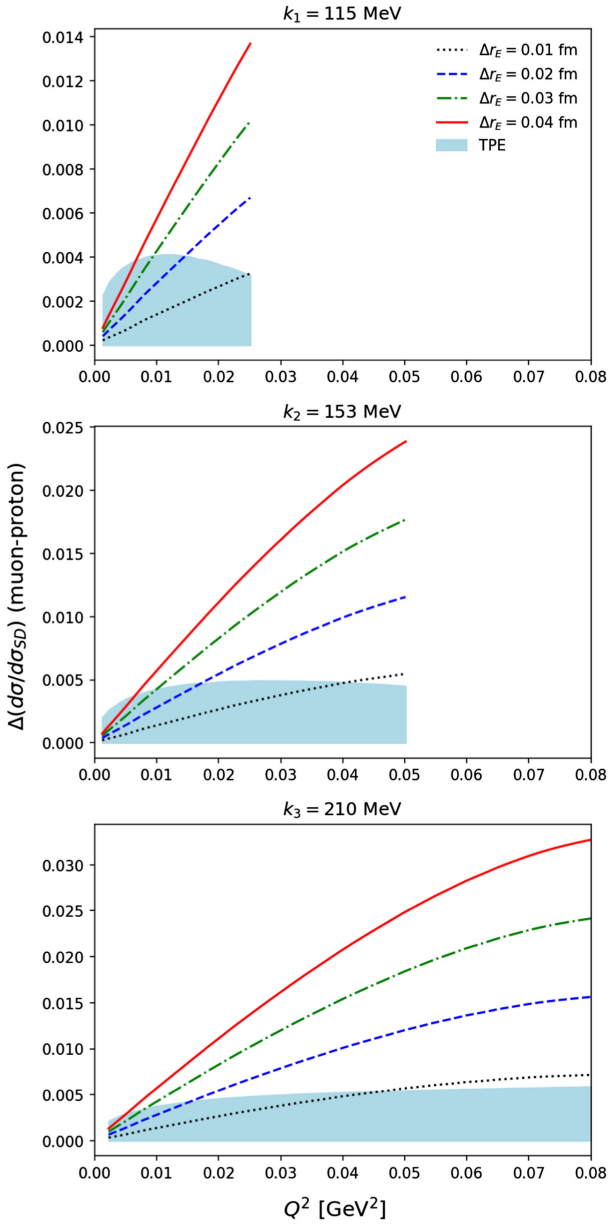


FIG. 6. Estimated accuracy of $\mu^- p$ cross section measurement required to discriminate between different values of the proton radius. Lines: Differences between DI$\chi$EFT cross section predictions for proton radii differing by $\Delta r_E$ (values see legend). Shaded band at bottom: Size of the TPE contribution [14].

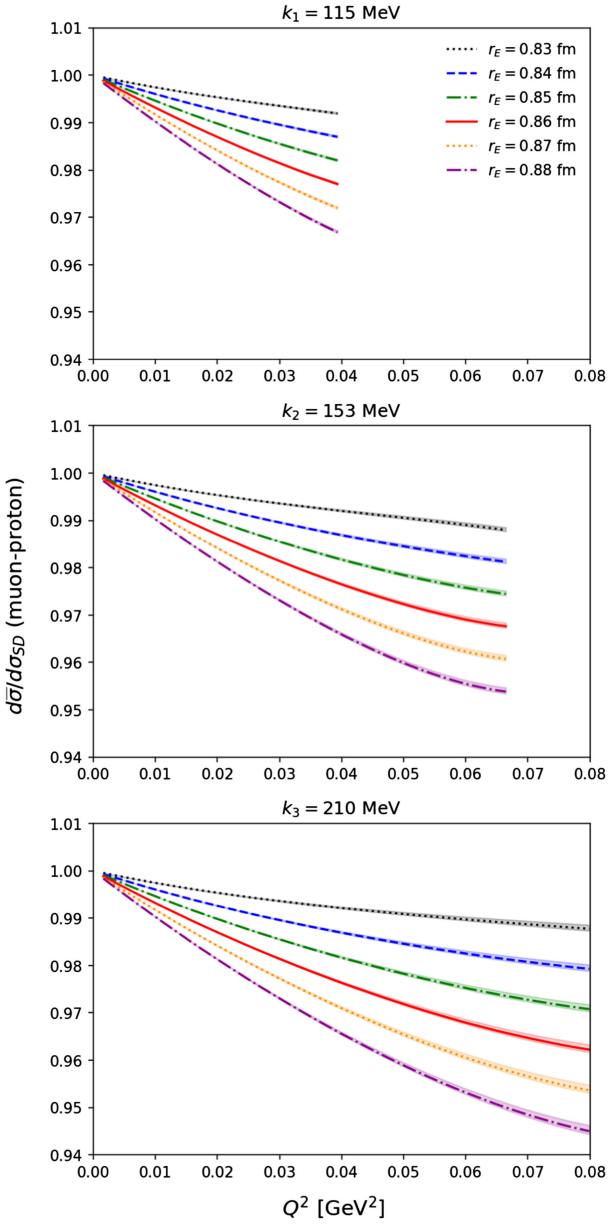


FIG. 7. DI$\chi$EFT predictions for the average of $\mu^+$ and $\mu^-$ elastic scattering cross sections Eq. (25) in MUSE kinematics, normalized to the standard dipole. Lines, shaded bands: Same notation as in Fig. 4.

for a given radius difference (note that the plots show the estimated total value of the TPE correction, not its uncertainty). The theoretical uncertainty of the TPE correction is not well known; however, we can assess how an assumed theoretical uncertainty of the TPE correction would impact on the overall uncertainty of the radius extraction. For the lowest beam momentum, $k = 115$ MeV, the size of the TPE correction is larger than the variation of the cross section prediction for $\Delta r_E = 0.01$ fm. The TPE correction thus has a decisive influence on the radius extraction in this kinematics. The situation becomes more favorable at higher beam momenta, where the TPE correction is comparable or smaller than the cross section variation for $\Delta r_E = 0.01$ fm.

Overall, our analysis suggests that the optimal kinematics for proton radius determination at MUSE with the DI$\chi$EFT method is at the highest beam momentum, $k = 210$ MeV, using momentum transfers $Q^2 \sim 0.05$–$0.08$ GeV$^2$, at the upper end of the experimentally accessible range. In this setting, the experimental precision required for radius determination with $\Delta r_E = 0.01$ fm is estimated at $\sim$0.8%. The final uncertainty of the radius extraction depends on the theoretical uncertainty of the TPE correction, which is not

known at present. An alternative method for proton radius extraction with $\mu p$ scattering uses the average of $\mu^+$ and $\mu^-$ cross sections,

$$\bar{\sigma} \equiv [\sigma(\mu^+ p) + \sigma(\mu^- p)]/2, \tag{25}$$

in which the TPE correction cancels due to its charge dependence. The same DI$\chi$EFT analysis of radius sensitivity and optimal kinematics as above can be performed in this case. The cross section prediction is now given by the one-photon exchange cross section Eq. (5). Figure 7 shows the predicted cross section and its theoretical uncertainty. The assessment of the optimal $Q^2$ values is the same as for $\mu^+ p$ above.

### C. Cross section prediction for nominal radius

The present study focuses on the prospects for extracting the proton radius from $\mu p$ scattering experiments at MUSE. The proton radius can also be extracted from atomic spectroscopy and $ep$ scattering experiments. In this context we can use DI$\chi$EFT to predict the $\mu p$ cross section expected for a given value of the radius and its theoretical uncertainty. For reference, we give here the prediction for the $\mu p$ cross section with the proton charge radius obtained in the previous DI$\chi$EFT analysis of $ep$ scattering results [9,10]

$$r_E = 0.842(2)\ \text{fm}. \tag{26}$$

Figure 8 shows the predicted $\mu^- p$ cross section in MUSE kinematics, Eq. (10), which includes the TPE correction; and the charge-averaged cross section, Eq. (25) in which the TPE correction cancels.

### D. Comparison of $ep$ and $\mu p$ scattering

It is interesting to compare the prospects for proton radius extraction in $ep$ and $\mu p$ scattering in the same kinematics. The MUSE experiment will measure both $ep$ and $\mu p$ scattering, and methods for proton radius extraction were studied intensively in earlier $ep$ scattering experiments. Characteristic differences between $ep$ and $\mu p$ occur in the TPE effects [14,24] and in the role of the magnetic FF. We exhibit them by repeating the DI$\chi$EFT analysis for $ep$ scattering and comparing with the $\mu p$ results.

Figure 9 shows the DI$\chi$EFT predictions for the $ep$ cross section for a range of assumed values of the proton radius, in the same style as Fig. 4 for $\mu p$. One observes: (a) The TPE corrections have different kinematic dependence in $ep$ than in $\mu p$ scattering [14,24]. In $ep$ they increase strongly with $Q^2$ at fixed $k$, and decrease with $k$ at fixed $Q^2$. In $\mu p$ the dependencies are much weaker. (b) The size of the TPE corrections relative to the variation of the cross section with the radius is much larger in $ep$ than in $\mu p$, especially at low beam momenta. At $k = 115$ MeV and $Q^2 = 0.02$ GeV$^2$,

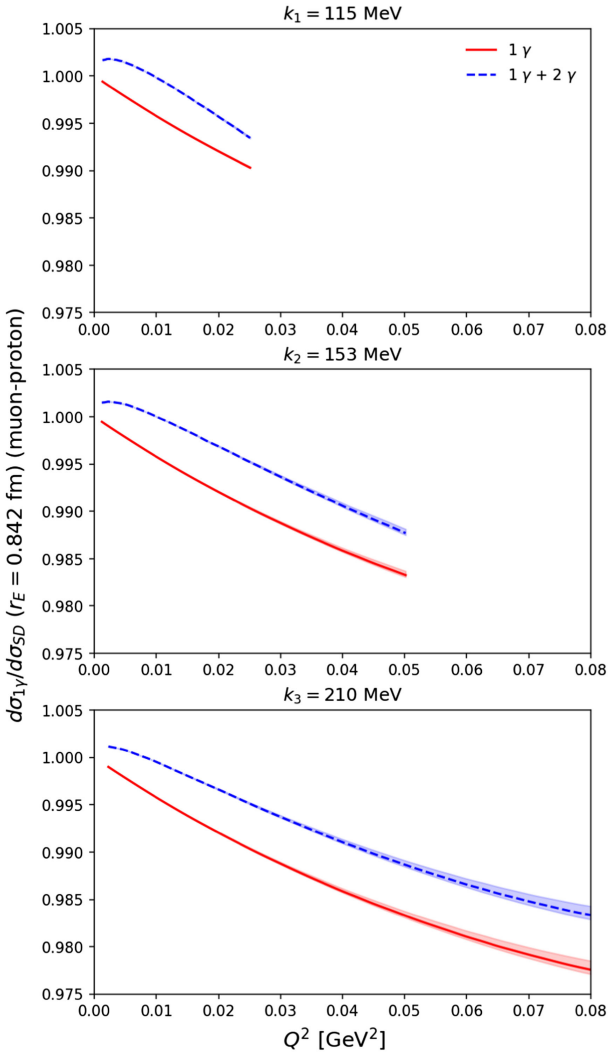


FIG. 8. DI$\chi$EFT predictions for $\mu p$ elastic scattering cross at MUSE for the nominal proton charge radius $r_E = 0.842(2)$ fm. Dashed line and shaded band (blue): $\mu^- p$ cross section, including one- and two-photon exchange contributions. Solid line and shaded band (red): Average of $\mu^+ p$ and $\mu^- p$ cross sections, given by the one-photon exchange contribution.

the size of the TPE correction amounts to a change of the radius $\Delta r_E \approx 0.03$ fm in $ep$ scattering, compared to $\Delta r_E \approx 0.015$ fm in $\mu p$ scattering in the same kinematics. (c) Overall, the different size and kinematic dependence of the TPE corrections causes a different $Q^2$-dependence of the cross section for $ep$ and $\mu p$ scattering at low $Q^2$.

Figure 10 shows the estimated accuracy of the $e^- p$ cross section measurement required for discriminating between different values of the radius, in the same style as Fig. 6 for $\mu^- p$. The optimal kinematics for radius extraction in $ep$ scattering at MUSE can be determined in the same way as for $\mu p$. The results of Fig. 10 show that the experimental accuracy required for radius extraction from $ep$ scattering is least at the highest beam momentum $k = 210$ MeV. The optimal $Q^2$ value determined by the trade-off between

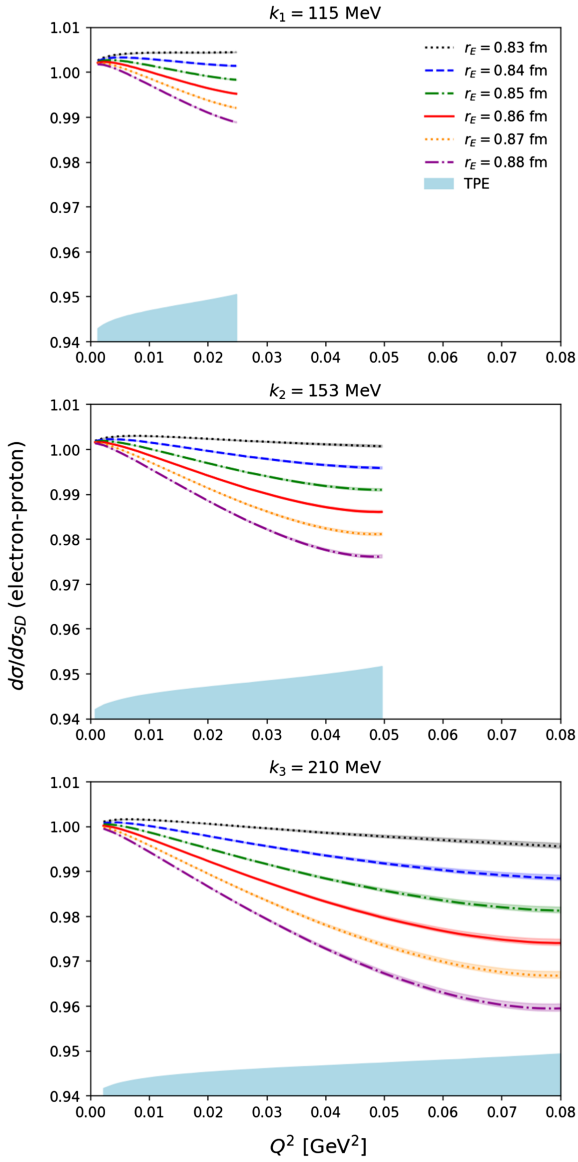


FIG. 9. DI$\chi$EFT predictions for the differential cross section of $ep$ scattering for several assumed value of the proton radius (compare with Fig. 4 for $\mu p$ scattering). The cross section predictions include the TPE correction and are normalized by the standard dipole cross section without TPE effects. Lines (solid, dashed, dotted, dashed-dotted): nominal DI$\chi$EFT predictions for the assumed value of the proton radius (see legend). Bands around lines: intrinsic theoretical uncertainty of DI$\chi$EFT prediction (unrelated to assumed proton radius). Blue band at bottom: TPE contribution to cross section [24].

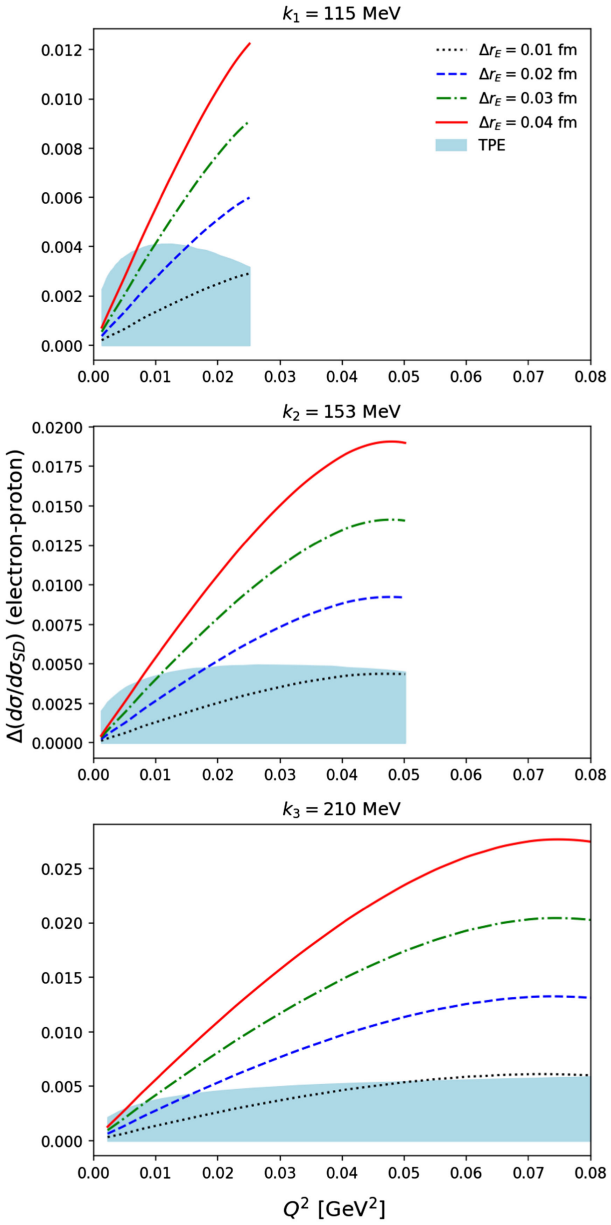


FIG. 10. Estimated accuracy of $e^- p$ cross section measurements required to discriminate between different values of the proton radius (compare with Fig. 6 for $\mu p$ scattering). Lines: differences between DI$\chi$EFT cross section predictions for proton radii differing by $\Delta r_E$ (values see legend). Shaded band at bottom: size of the TPE contribution [24].

radius sensitivity and theoretical uncertainty is at $Q^2 \sim 0.065$ GeV$^2$, slightly below the kinematic limit.

Figure 11 shows the ratio of the $\mu p$ to $ep$ cross sections (including the TPE corrections) for the same set of assumed proton radii. The ratio directly expresses the different $Q^2$-dependence of the $ep$ and $\mu p$ cross sections. Its magnitude and $Q^2$-dependence are determined by the kinematic factors in the one-photon-exchange cross section Eq. (5) et seq. One observes that the ratio is remarkably insensitive to the proton charge radius in this kinematic regime, especially at the lower values of $k$. Only at $k =$ 210 MeV the differences between the radii become visible at the largest $Q^2$ values.

The results of Fig. 9 show that the TPE corrections play a much larger role in proton radius extraction from $ep$ scattering than $\mu p$ scattering, and that they limit the theoretical uncertainty of the extracted radius. With the

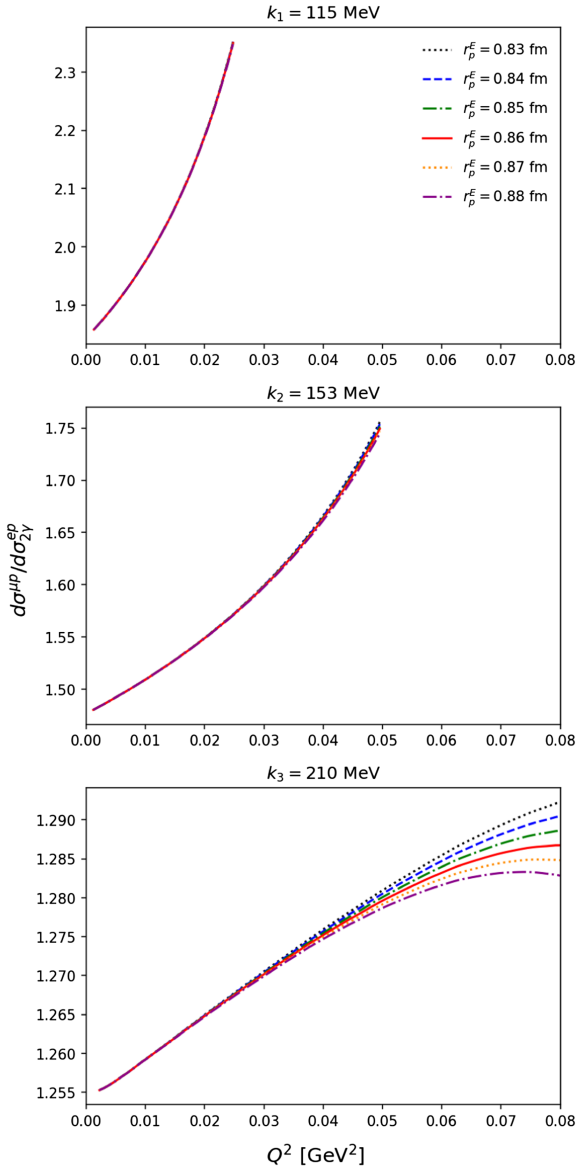


FIG. 11. DI$\chi$EFT predictions of the ratio of $\mu p$ to $ep$ elastic scattering cross sections $\sigma$, Eq. (10), including the TPE corrections, for several assumed values of the proton radius.

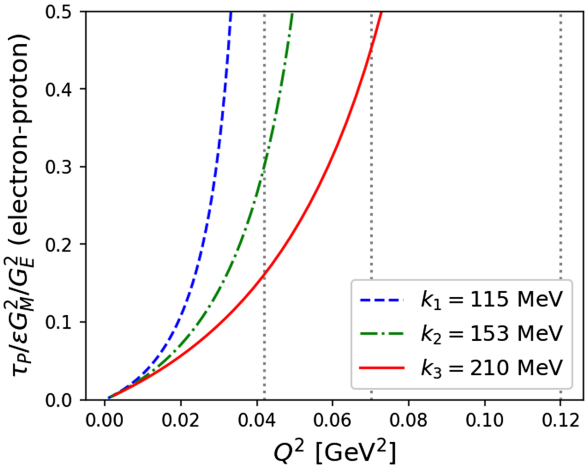


FIG. 12. Ratio of magnetic and electric contributions to the $ep$ elastic scattering cross section, $(\tau_P/\epsilon)G_M^2/G_E^2$, in MUSE kinematics (compare with Fig. 5 for $\mu p$ scattering). The vertical dotted lines represent the kinematic upper limits of $Q^2$ at the given beam momentum $k$, Eq. (4).

DI$\chi$EFT method, the influence of TPE corrections in $ep$ can be minimized by using the data at the highest beam momentum $k = 210$ MeV and momentum transfers in the range $Q^2 \sim 0.03$–$0.08$ GeV$^2$ for radius extraction. In this kinematics the cross section shows good sensitivity to the proton charge radius, the theoretical uncertainty of the DI$\chi$EFT predictions is small, and the size of the TPE corrections amounts to a shift of the radius $\Delta r_E \sim 0.01$ fm (see Fig. 9). The ability to recruit higher-$Q^2$ data for radius extraction with DI$\chi$EFT is thus even more advantageous in $ep$ than in $\mu p$ scattering.

An important difference between $ep$ and $\mu p$ scattering appears in the contribution of the magnetic FF at large momentum transfers, at the upper end of the allowed kinematic range. In $ep$ scattering $\epsilon = 0$ at $Q^2 \sim Q^2_{\rm max}$ (if one neglects the electron mass), while in $\mu p$ scattering $\epsilon$ attains a finite value, see Eq. (9). In $ep$ scattering the one-photon exchange cross section for $Q^2 \to Q^2_{\rm max}$ is therefore dominated by $G_M$. Figure 12 shows the ratio of magnetic and electric contributions to the one-photon-exchange cross section for $ep$ scattering, in the same way as Fig. 5 for $\mu p$. One sees that the magnetic contribution to the cross section is substantially larger in $ep$ than $\mu p$ already for $Q^2$ in the middle of the kinematic range. This circumstance must be taken into account when assessing the sensitivity of the cross section to $r_E$ in DI$\chi$EFT, and one should remain in the region where the cross section is not dominated by $G_M$. We have quantified the impact of the uncertainty in $G_M$ on the proton radius extraction from $ep$ scattering in the same way as for $\mu p$ (see Sec. III A), using the DI$\chi$EFT framework and the experimental uncertainty of $G_M$ obtained in an earlier analysis [9]. We find that the current experimental uncertainty of $G_M$ produces a relative variation of the cross section of at most $\sim$0.05% in the range covered by Fig. 9. The uncertainty from $G_M$ is thus not a limiting factor of the DI$\chi$EFT-based radius extraction from $ep$ scattering data in MUSE kinematics.

Because of the large TPE corrections in $ep$ scattering, it would be an attractive option to perform the proton radius extraction with the average of $e^- p$ and $e^+ p$ cross sections [see Eq. (25) for $\mu^\pm p$], in which the TPE effects cancel. In this case the cross section is accurately described by the one-photon-exchange formula, and the analysis greatly simplifies. Figure 13 shows the DI$\chi$EFT predictions for the charge radius dependence of the charge-averages cross section $\bar{\sigma}$ in $e^\pm p$ scattering in MUSE kinematics.

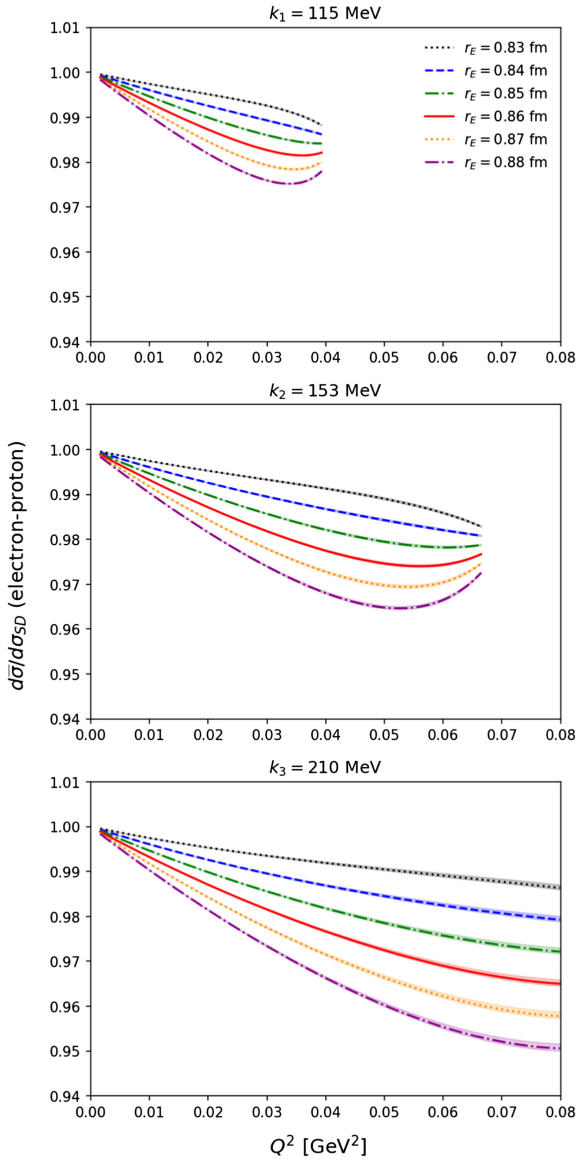


FIG. 13. DI$\chi$EFT predictions for the average of $e^+$ and $e^-$ elastic scattering cross sections, as in Eq. (25) for $\mu^+p$ and $\mu^-p$, in MUSE kinematics (compare with Fig. 7 for $\mu p$ scattering).

## IV. CONCLUSIONS

In this work we have used the DI$\chi$EFT framework to study the prospects for the proton radius extraction from $\mu p$ scattering at MUSE. The principal conclusions are

(i) When extracting the radius from fits to cross section data at low momentum transfers $Q^2 < 0.01$ GeV$^2$, the TPE corrections need to be included with high precision. At $Q^2 < 0.01$ GeV$^2$, the estimated absolute size of TPE correction amounts to a shift of the extracted radius by 0.03–0.04 fm. Any theoretical uncertainty of the TPE correction will influence the extracted radius proportionally.

(ii) The DI$\chi$EFT method allows one to extract the radius from fits to cross section data at higher momentum transfers $Q^2\sim$ few times 0.01 GeV$^2$ in the MUSE kinematic range. This is advantageous experimentally, because the higher sensitivity of the cross section to the radius lowers the demands on the experimental precision of the cross section measurement. It is also advantageous theoretically, as it reduces the influence of the TPE correction on the radius extraction.

(iii) The optimal kinematics for the DI$\chi$EFT-based radius extraction at MUSE is $k = 210$ MeV and $Q^2 \sim 0.05$–$0.08$ GeV$^2$, at the upper end of the kinematic coverage. It is determined by the trade-off between theoretical effects—the sensitivity of the cross section to the radius, the uncertainty of the DI$\chi$EFT FF predictions, and the TPE correction. In this kinematics, even a 100% uncertainty of the TPE correction would shift the extracted radius only by 0.01 fm. An experimental precision of $\lesssim 0.5\%$ is required for determining the radius with 0.01 fm accuracy. Such accuracy would be sufficient for solving the proton radius puzzle.

(iv) In $ep$ scattering in MUSE kinematics, the TPE corrections are generally larger that in $\mu p$, and the advantages of using the DI$\chi$EFT method with higher-$Q^2$ data for radius extraction are even more compelling. The ratio of same-charge $ep$ and $\mu p$ cross sections is predicted to be practically independent of the proton radius and can be used for validation of the analysis.

Our findings affirm the need for accurate theoretical estimates of the TPE corrections in elastic $\mu p$ and $ep$ scattering. If the radius extraction is performed using the DI$\chi$EFT framework and data at finite momentum transfers $Q^2 \sim 0.05$–$0.08$ GeV$^2$, as recommended here, efforts should focus on improving the TPE estimates in this kinematic region. At these finite values of $Q^2$ the constraints on the TPE amplitude from the limit of forward scattering ($Q^2 = 0$) are less restrictive, and the calculations become more dependent on dynamical assumptions [14,24]. Methods based on the $1/N_c$ expansion of QCD could enable systematic calculations of TPE effects with controlled theoretical uncertainties; see Refs. [25,26] for recent developments.

The DI$\chi$EFT framework used in the present study is a general method that can be improved through further development. In particular, the treatment of the high-mass states in the spectral function can be chosen depending on the $Q^2$ range and the required accuracy. In this work we have used simple effective parametrizations of the high-mass spectral function and treated the functional form as a theoretical uncertainty, which is sufficient for the present analysis in the MUSE $Q^2$-range (see Sec. II B). The uncertainty could be reduced by using more elaborate parametrizations of the high-mass spectral function and constraining it with FF data at larger $Q^2 \lesssim 1$ GeV$^2$. This

would allow one to include higher-$Q^2$ data in the DI$\chi$EFT-based radius extraction.

## ACKNOWLEDGMENTS

We thank A. Gramolin for making available a computer code that was used to validate the numerical calculation of the one-photon exchange cross section, and P. Blunden and W. Melnitchouk for helpful correspondence about two-photon exchange effects. J. M. A. acknowledges support from the Spanish MICINN Grant No. PID2019–106080 GB-C21. This material is based upon work supported by the U.S. Department of Energy, Office of Science, Office of Nuclear Physics under Contract No. DE-AC05-06OR23177.

[1] G. A. Miller, Defining the proton radius: A unified treatment, Phys. Rev. C **99**, 035202 (2019).
[2] R. Pohl *et al.*, The size of the proton, Nature (London) **466**, 213 (2010).
[3] P. J. Mohr, B. N. Taylor, and D. B. Newell, CODATA recommended values of the fundamental physical constants: 2006, Rev. Mod. Phys. **80**, 633 (2008).
[4] R. Pohl, R. Gilman, G. A. Miller, and K. Pachucki, Muonic hydrogen and the proton radius puzzle, Annu. Rev. Nucl. Part. Sci. **63**, 175 (2013).
[5] C. E. Carlson, The proton radius puzzle, Prog. Part. Nucl. Phys. **82**, 59 (2015).
[6] R. Gilman *et al.* (MUSE Collaboration), Technical design report for the Paul Scherrer Institute Experiment R-12-01.1: Studying the proton "Radius" puzzle with $\mu p$ elastic scattering, arXiv:1709.09753.
[7] J. M. Alarcón and C. Weiss, Nucleon form factors in dispersively improved chiral effective field theory II: Electromagnetic form factors, Phys. Rev. C **97**, 055203 (2018).
[8] J. M. Alarcón and C. Weiss, Accurate nucleon electromagnetic form factors from dispersively improved chiral effective field theory, Phys. Lett. B **784**, 373 (2018).
[9] J. M. Alarcón, D. W. Higinbotham, and C. Weiss, Precise determination of the proton magnetic radius from electron scattering data, Phys. Rev. C **102**, 035203 (2020).
[10] J. M. Alarcón, D. W. Higinbotham, C. Weiss, and Z. Ye, Proton charge radius extraction from electron scattering data using dispersively improved chiral effective field theory, Phys. Rev. C **99**, 044303 (2019).
[11] O. Tomalak and M. Vanderhaeghen, Dispersion relation formalism for the two-photon exchange correction to elastic muon–proton scattering: Elastic intermediate state, Eur. Phys. J. C **78**, 514 (2018).
[12] C. E. Carlson and M. Vanderhaeghen, Two-photon physics in hadronic processes, Annu. Rev. Nucl. Part. Sci. **57**, 171 (2007).
[13] J. Arrington, P. G. Blunden, and W. Melnitchouk, Review of two-photon exchange in electron scattering, Prog. Part. Nucl. Phys. **66**, 782 (2011).
[14] O. Tomalak and M. Vanderhaeghen, Two-photon exchange correction to muon–proton elastic scattering at low momentum transfer, Eur. Phys. J. C **76**, 125 (2016).
[15] P. Talukdar, V. C. Shastry, U. Raha, and F. Myhrer, Lepton-proton two-photon exchange in chiral perturbation theory, Phys. Rev. D **101**, 013008 (2020).
[16] P. Talukdar, V. C. Shastry, U. Raha, and F. Myhrer, Radiative and chiral corrections to elastic lepton-proton scattering in chiral perturbation theory, Phys. Rev. D **104**, 053001 (2021).
[17] X.-H. Cao, Q.-Z. Li, and H.-Q. Zheng, Radiative correction to lepton proton scatterings in manifestly Lorentz-invariant chiral perturbation theory, Phys. Rev. D **105**, 094008 (2022).
[18] J. M. Alarcón and C. Weiss, Nucleon form factors in dispersively improved chiral effective field theory: Scalar form factor, Phys. Rev. C **96**, 055206 (2017).
[19] J. M. Alarcón and C. Weiss, Transverse charge and current densities in the nucleon from dispersively improved chiral effective field theory, Phys. Rev. D **106**, 054005 (2022).
[20] G. Hohler, E. Pietarinen, I. Sabba Stefanescu, F. Borkowski, G. G. Simon, V. H. Walther, and R. D. Wendling, Analysis of electromagnetic nucleon form-factors, Nucl. Phys. **B114**, 505 (1976).
[21] M. A. Belushkin, H. W. Hammer, and U. G. Meissner, Dispersion analysis of the nucleon form-factors including meson continua, Phys. Rev. C **75**, 035202 (2007).
[22] I. Lorenz, H.-W. Hammer, and U.-G. Meissner, The size of the proton—closing in on the radius puzzle, Eur. Phys. J. A **48**, 151 (2012).
[23] M. Hoferichter, B. Kubis, J. Ruiz de Elvira, H. W. Hammer, and U. G. Meißner, On the $\pi\pi$ continuum in the nucleon form factors and the proton radius puzzle, Eur. Phys. J. A **52**, 331 (2016).
[24] O. Tomalak and M. Vanderhaeghen, Two-photon exchange correction in elastic unpolarized electron-proton scattering at small momentum transfer, Phys. Rev. D **93**, 013023 (2016).
[25] J. L. Goity, C. Weiss, and C. T. Willemyns, Target normal single-spin asymmetry in inclusive electron-nucleon scattering with two-photon exchange: Analysis using $1/N_c$ expansion, Phys. Lett. B **835**, 137580 (2022).
[26] J. L. Goity, C. Weiss, and C. Willemyns, Target normal single-spin asymmetry in inclusive electron-nucleon scattering in the $1/N_c$ expansion, Phys. Rev. D **107**, 094026 (2023).